

April 2018

Renormalization on the fuzzy sphere

Kohta HATAKEYAMA^{1,2)*}, Asato TSUCHIYA^{1,2)†} AND Kazushi YAMASHIRO^{1)‡}

¹⁾ *Department of Physics, Shizuoka University
836 Ohya, Suruga-ku, Shizuoka 422-8529, Japan*

²⁾ *Graduate School of Science and Technology, Shizuoka University
3-5-1 Johoku, Naka-ku, Hamamatsu 432-8011, Japan*

Abstract

We study renormalization on the fuzzy sphere. We numerically simulate a scalar field theory on it, which is described by a Hermitian matrix model. We show that correlation functions defined by using the Berezin symbol are made independent of the matrix size, which is viewed as a UV cutoff, by tuning a parameter of the theory. We also find that the theories on the phase boundary are universal. They behave as a conformal field theory at short distances, while they show an effect of UV/IR mixing at long distances.

* e-mail address : hatakeyama.kohta.15@shizuoka.ac.jp

† e-mail address : tsuchiya.asato@shizuoka.ac.jp

‡ e-mail address : yamashiro.kazushi.17@shizuoka.ac.jp

1 Introduction

A lot of attention has been paid to field theories on noncommutative spaces, mainly because they have a deep connection to string theory or quantum gravity (for a review, see [1]). One of the most peculiar phenomena in field theories on noncommutative spaces is the so-called UV/IR mixing [2]. This is known to be an obstacle to perturbative renormalization.

In [3,4], the UV/IR mixing in a scalar field theory on the fuzzy sphere¹, which is realized by a matrix model, was examined perturbatively: the one-loop self-energy differs from that in the ordinary theory on a sphere by finite and non-local terms even in the commutative limit. This effect is sometimes called the UV/IR anomaly.

It is important to elucidate the problem of renormalization to construct consistent quantum field theories on noncommutative spaces. It was shown in [10] by Monte Carlo study that by tuning the mass parameter the 2-point and 4-point correlation functions in the disordered phase of the above theory are made independent of the matrix size up to a wave function renormalization, where the matrix size is interpreted as a UV cutoff². This strongly suggests that the theory is nonperturbatively renormalizable in the disordered phase.

In this paper, we perform further study of the scalar field theory on the fuzzy sphere by Monte Carlo simulation. We define the correlation functions by using the Berezin symbol [22] as in [10]. First, we show that the 2-point and 4-point correlation functions are made independent of the matrix size by tuning the coupling constant. Thus, we verify a conjecture in [10] that the theory is universal up to a parameter fine-tuning. Next, we identify the phase boundary by measuring the susceptibility that is an order parameter for the Z_2 symmetry and calculate the 2-point and 4-point correlation functions on the boundary. We find that the correlation functions at different points on the boundary agree so that the theories on the boundary are universal as in ordinary field theories. Furthermore, we observe that the 2-point correlation functions behave as those in a conformal field theory (CFT) at short distances but deviate from it at long distances. It is nontrivial that the behavior of the CFT is seen because field theories on noncommutative spaces are non-local ones.

This paper is organized as follows. In section 2, we introduce the scalar field theory

¹The theory has been studied by Monte Carlo simulation in [5–10]. For related analytic studies of the model, see [11–19].

²A similar analysis for a scalar field theory on the noncommutative torus was performed in [20,21]

on the fuzzy sphere and review its connection to the theory on a sphere. In section 3, we study renormalization in the disordered phase. In section 4, we identify the phase boundary and calculate the 2-point and 4-point correlation functions on the boundary. Section 5 is devoted to the conclusion and discussion. In the appendix, we review the Bloch coherent state and the Berezin symbol.

2 Scalar field theory on the fuzzy sphere

Throughout this paper, we examine the following matrix model:

$$S = \frac{1}{N} \text{Tr} \left(-\frac{1}{2} [L_i, \Phi]^2 + \frac{\mu^2}{2} \Phi^2 + \frac{\lambda}{4} \Phi^4 \right) , \quad (2.1)$$

where Φ is an $N \times N$ Hermitian matrix, and L_i ($i = 1, 2, 3$) are the generators of the $SU(2)$ algebra with the spin- $(N - 1)/2$ representation, which obey the commutation relation

$$[L_i, L_j] = i\epsilon_{ijk} L_k . \quad (2.2)$$

The theory possesses Z_2 symmetry: $\Phi \rightarrow -\Phi$. The path-integral measure is given by $d\Phi e^{-S}$, where

$$d\Phi = \prod_{i=1}^N d\Phi_{ii} \prod_{1 \leq j < k \leq N} d\text{Re}\Phi_{jk} d\text{Im}\Phi_{jk} . \quad (2.3)$$

The theory (2.1) reduces to the following continuum theory on a sphere with the radius R at the tree level in the $N \rightarrow \infty$ limit, which corresponds to the so-called commutative limit:

$$S_c = \frac{R^2}{4\pi} \int d\Omega \left(-\frac{1}{2R^2} (\mathcal{L}_i \phi)^2 + \frac{m^2}{2} \phi^2 + \frac{g}{4} \phi^4 \right) , \quad (2.4)$$

where $d\Omega$ is the invariant measure on the sphere and \mathcal{L}_i ($i = 1, 2, 3$) are the orbital angular momentum operators. The correspondence of the parameters in (2.1) and (2.4) is given by

$$\begin{aligned} \mu^2 &= R^2 m^2 , \\ \lambda &= R^2 g . \end{aligned} \quad (2.5)$$

We review the above tree-level correspondence in the appendix. It was shown in [3, 4] that there exist finite differences between (2.1) and (2.4) in the perturbative expansion, which are known as the UV/IR anomaly.

To define correlation functions, we introduce the Berezin symbol [22] that is constructed from the Bloch coherent state [23]. We parametrize the sphere in terms of the standard polar coordinates $\Omega = (\theta, \varphi)$. The Bloch coherent state $|\Omega\rangle$ is localized around the point (θ, φ) with the width R/\sqrt{N} . The Berezin symbol for an $N \times N$ matrix A is given by $\langle \Omega|A|\Omega\rangle$. The Berezin symbol $\langle \Omega|\Phi|\Omega\rangle$ is identified with the field $\phi(\Omega)$ in the correspondence at the tree level between (2.1) and (2.4). The Bloch coherent state and the Berezin symbol are reviewed in the appendix.

3 Correlation functions

3.1 Definition of correlation functions

By denoting the Berezin symbol briefly as

$$\varphi(\Omega) = \langle \Omega|\Phi|\Omega\rangle , \quad (3.1)$$

we define the n -point correlation function in the theory (2.1) as

$$\langle \varphi(\Omega_1)\varphi(\Omega_2)\cdots\varphi(\Omega_n)\rangle = \frac{\int d\Phi \varphi(\Omega_1)\varphi(\Omega_2)\cdots\varphi(\Omega_n) e^{-S}}{\int d\Phi e^{-S}} . \quad (3.2)$$

The correlation function (3.2) is a counterpart of $\langle \phi(\Omega_1)\phi(\Omega_2)\cdots\phi(\Omega_n)\rangle$ in the theory (2.4).

We assume that the matrix Φ in (2.1) is renormalized as

$$\Phi = \sqrt{Z}\Phi_r , \quad (3.3)$$

where Φ_r is the renormalized matrix. Then, we define the renormalized Berezin symbol $\varphi_r(\Omega)$ by

$$\varphi(\Omega) = \sqrt{Z}\varphi_r(\Omega) , \quad (3.4)$$

and the renormalized n -point correlation function $\langle \varphi_r(\Omega_1)\varphi_r(\Omega_2)\cdots\varphi_r(\Omega_n)\rangle$ by

$$\langle \varphi(\Omega_1)\varphi(\Omega_2)\cdots\varphi(\Omega_n)\rangle = Z^{\frac{n}{2}} \langle \varphi_r(\Omega_1)\varphi_r(\Omega_2)\cdots\varphi_r(\Omega_n)\rangle . \quad (3.5)$$

In the following, we calculate the following correlation functions:

$$\begin{aligned} & \text{1-point function: } \langle \varphi(\Omega_1)\rangle , \\ & \text{2-point function: } \langle \varphi(\Omega_p)\varphi(\Omega_q)\rangle \quad (1 \leq p < q \leq 4) , \\ & \text{4-point function: } \langle \varphi(\Omega_1)\varphi(\Omega_2)\varphi(\Omega_3)\varphi(\Omega_4)\rangle . \end{aligned} \quad (3.6)$$

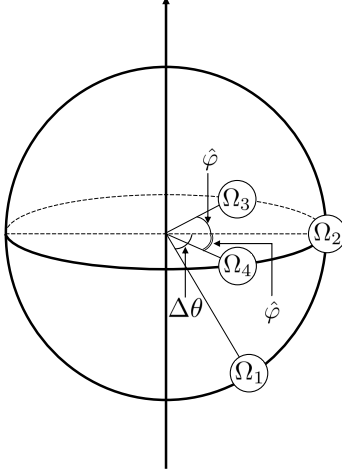


Figure 1: Four points on the sphere chosen for the correlation functions.

We verify that the 1-point functions vanish in the parameter region that we examine in this section. This implies that we work in the disordered phase. Thus, the 2-point correlation functions are themselves the connected ones, while the connected 4-point correlation functions are given by

$$\begin{aligned} \langle \varphi(\Omega_1)\varphi(\Omega_2)\varphi(\Omega_3)\varphi(\Omega_4) \rangle_c &= \langle \varphi(\Omega_1)\varphi(\Omega_2)\varphi(\Omega_3)\varphi(\Omega_4) \rangle - \langle \varphi(\Omega_1)\varphi(\Omega_2) \rangle \langle \varphi(\Omega_3)\varphi(\Omega_4) \rangle \\ &\quad - \langle \varphi(\Omega_1)\varphi(\Omega_3) \rangle \langle \varphi(\Omega_2)\varphi(\Omega_4) \rangle - \langle \varphi(\Omega_1)\varphi(\Omega_4) \rangle \langle \varphi(\Omega_2)\varphi(\Omega_3) \rangle , \end{aligned} \quad (3.7)$$

where c stands for the connected part. The renormalized correlation functions are defined as

$$\langle \varphi(\Omega_1) \rangle = \sqrt{Z} \langle \varphi_r(\Omega_1) \rangle , \quad (3.8)$$

$$\langle \varphi(\Omega_p)\varphi(\Omega_q) \rangle = Z \langle \varphi_r(\Omega_p)\varphi_r(\Omega_q) \rangle , \quad (3.9)$$

$$\langle \varphi(\Omega_1)\varphi(\Omega_2)\varphi(\Omega_3)\varphi(\Omega_4) \rangle_c = Z^2 \langle \varphi_r(\Omega_1)\varphi_r(\Omega_2)\varphi_r(\Omega_3)\varphi_r(\Omega_4) \rangle_c . \quad (3.10)$$

We pick up four points $\Omega_p = (\theta_p, \varphi_p)$ ($p = 1, 2, 3, 4$) on the sphere as follows (see Fig. 1):

$$\begin{aligned} \Omega_1 &= \left(\frac{\pi}{2} + \Delta\theta, 0 \right) , \\ \Omega_2 &= \left(\frac{\pi}{2}, 0 \right) , \\ \Omega_3 &= \left(\frac{\pi}{2}, \hat{\varphi} \right) , \\ \Omega_4 &= \left(\frac{\pi}{2}, -\hat{\varphi} \right) , \end{aligned} \quad (3.11)$$

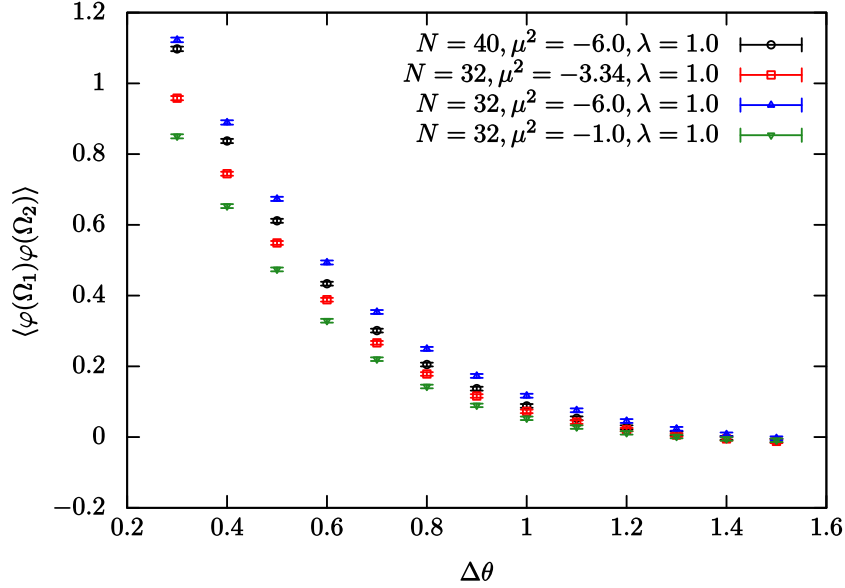


Figure 2: $\langle \varphi(\Omega_1)\varphi(\Omega_2) \rangle$ at $\lambda = 1.0$ is plotted against $\Delta\theta$. Circles represent the data for $N = 40$ and $\mu^2 = -6.0$, while squares, triangles, and inverted triangles represent the data for $N = 32$ and $\mu^2 = -3.34, -6.0, -1.0$, respectively.

where $\hat{\varphi} = \pi/12$ and $\Delta\theta = 0.1m$ with m taken from 1 to 15.

We apply the hybrid Monte Carlo method to our simulation of the theory.

3.2 Tuning μ^2

In this subsection, we renormalize the theory by tuning μ^2 . We fix λ at 1.0.

First, we simulate at $N = 40$ and $\mu^2 = -6.0$. Then, we simulate at $N = 32$ for various values of μ^2 . In Fig.2, we plot

$$\langle \varphi(\Omega_1)\varphi(\Omega_2) \rangle = Z \langle \varphi_r(\Omega_1)\varphi_r(\Omega_2) \rangle \quad (3.12)$$

against $\Delta\theta$ at $N = 40$ and $\mu^2 = -6.0$ and at $N = 32$ and typical values of μ^2 , $-6.0, -3.34, -1.0$.

We find that the data for $N = 32$ and $\mu^2 = -3.34$ agree with the ones for $N = 40$ and $\mu^2 = -6.0$ if the former are multiplied by a constant and that this is not the case for the data for $N = 32$ and $\mu^2 = -6.0, -1.0$. We determined the above constant as $\zeta_{32 \rightarrow 40} = \frac{Z(40)}{Z(32)} = 1.263(8)$ by using the least-squares method. In Fig.3, we plot $\langle \varphi(\Omega_1)\varphi(\Omega_2) \rangle$ at $N = 40$ and $\mu^2 = -6.0$ and $\zeta_{32 \rightarrow 40} \langle \varphi(\Omega_1)\varphi(\Omega_2) \rangle$ at $N = 32$ and $\mu^2 = -3.34$ against $\Delta\theta$. We indeed see that the data for $N = 32$ agree nicely with the ones for $N = 40$. This implies that the renormalized 2-point functions at $N = 32$ and $N = 40$ agree.

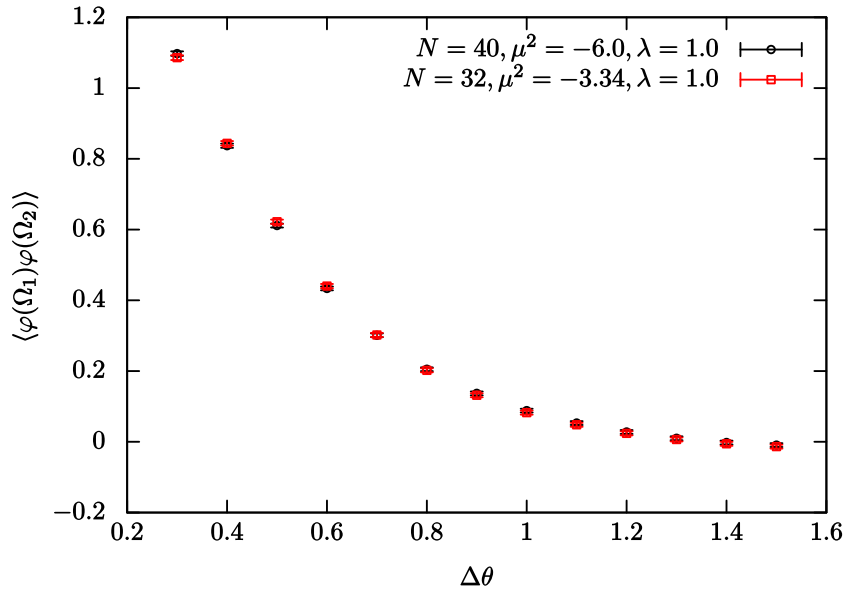


Figure 3: $\langle \varphi(\Omega_1)\varphi(\Omega_2) \rangle$ at $N = 40$, $\mu^2 = -6.0$, and $\lambda = 1.0$ is plotted against $\Delta\theta$ (circles). $\zeta_{32 \rightarrow 40} \langle \varphi(\Omega_1)\varphi(\Omega_2) \rangle$ with $\zeta_{32 \rightarrow 40} = 1.263(8)$ at $N = 32$, $\mu^2 = -3.34$, and $\lambda = 1.0$ is also plotted against $\Delta\theta$ (squares).

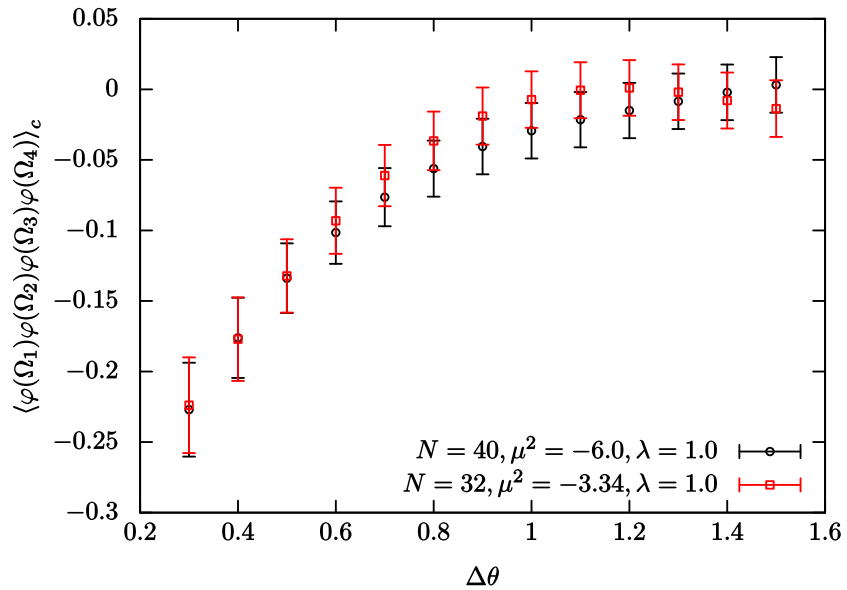


Figure 4: $\langle \varphi(\Omega_1)\varphi(\Omega_2)\varphi(\Omega_3)\varphi(\Omega_4) \rangle_c$ at $N = 40$, $\mu^2 = -6.0$, and $\lambda = 1.0$ is plotted against $\Delta\theta$ (circles). $\zeta_{32 \rightarrow 40}^2 \langle \varphi(\Omega_1)\varphi(\Omega_2)\varphi(\Omega_3)\varphi(\Omega_4) \rangle_c$ with $\zeta_{32 \rightarrow 40}^2 = 1.595$ at $N = 32$, $\mu^2 = -3.34$, and $\lambda = 1.0$ is also plotted against $\Delta\theta$ (squares).

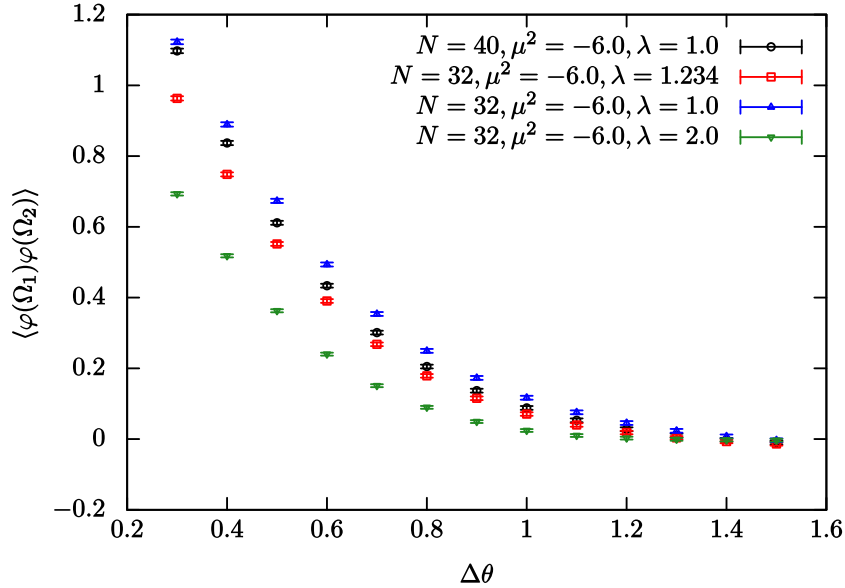


Figure 5: $\langle \varphi(\Omega_1)\varphi(\Omega_2) \rangle$ at $\mu^2 = -6.0$ is plotted against $\Delta\theta$. Circles represent the data for $N = 40$ and $\lambda = 1.0$, while squares, triangles, and inverted triangles represent the data for $N = 32$ and $\lambda = 1.234, 1.0, 2.0$, respectively.

Furthermore, in Fig.4, we plot $\langle \varphi(\Omega_1)\varphi(\Omega_2)\varphi(\Omega_3)\varphi(\Omega_4) \rangle_c$ at $N = 40$ and $\mu^2 = -6.0$ and $\zeta_{32 \rightarrow 40}^2 \langle \varphi(\Omega_1)\varphi(\Omega_2)\varphi(\Omega_3)\varphi(\Omega_4) \rangle_c$ at $N = 32$ and $\mu^2 = -3.34$ against $\Delta\theta$. We again see a nice agreement between the data for $N = 32$ and the ones for $N = 40$, which means that the renormalized connected 4-point functions at $N = 32$ agree with those at $N = 40$. We do not see the above agreement of the correlation functions for $m = 1, 2$ in (3.11). We consider this to be attributed to the UV cutoff.

The above results strongly suggest that the correlation functions are made independent of N up to a wave function renormalization by tuning μ^2 and that the theory is nonperturbatively renormalizable in the ordinary sense.

3.3 Tuning λ

In this subsection, we renormalize the theory by tuning λ . We fix μ^2 at -6.0 .

We simulate at $N = 32$ for various values of λ . In Fig.5, we plot

$$\langle \varphi(\Omega_1)\varphi(\Omega_2) \rangle = Z \langle \varphi_r(\Omega_1)\varphi_r(\Omega_2) \rangle \quad (3.13)$$

against $\Delta\theta$ at $N = 40$ and $\lambda = 1.0$ and at $N = 32$ and typical values of λ , 1.0, 1.234, 2.0. We find that the data for $N = 32$ and $\lambda = 1.234$ agree with the ones for $N = 40$ and

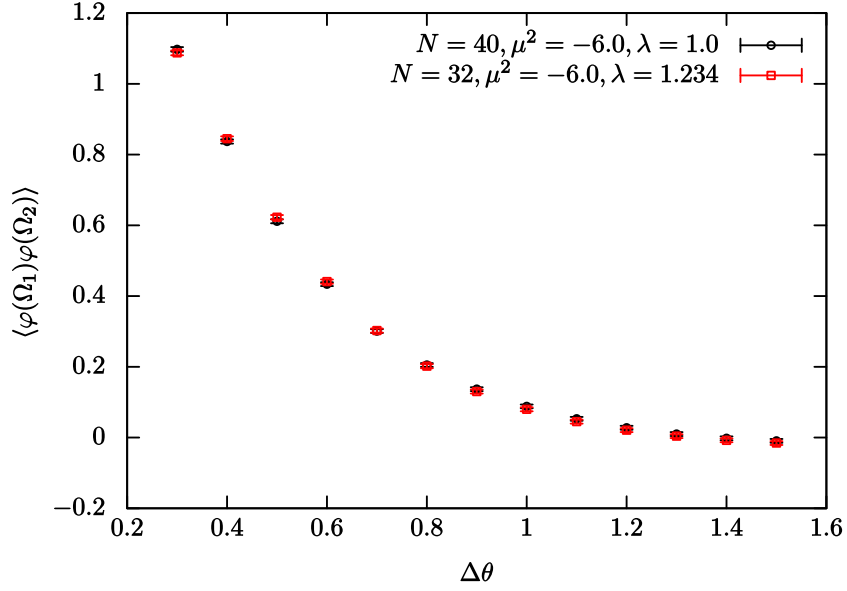


Figure 6: $\langle \varphi(\Omega_1)\varphi(\Omega_2) \rangle$ at $N = 40$, $\mu^2 = -6.0$, and $\lambda = 1.0$ is plotted against $\Delta\theta$ (circles). $\zeta'_{32 \rightarrow 40} \langle \varphi(\Omega_1)\varphi(\Omega_2) \rangle$ with $\zeta'_{32 \rightarrow 40} = 1.129(8)$ at $N = 32$, $\mu^2 = -6.0$, and $\lambda = 1.234$ is also plotted against $\Delta\theta$ (squares).

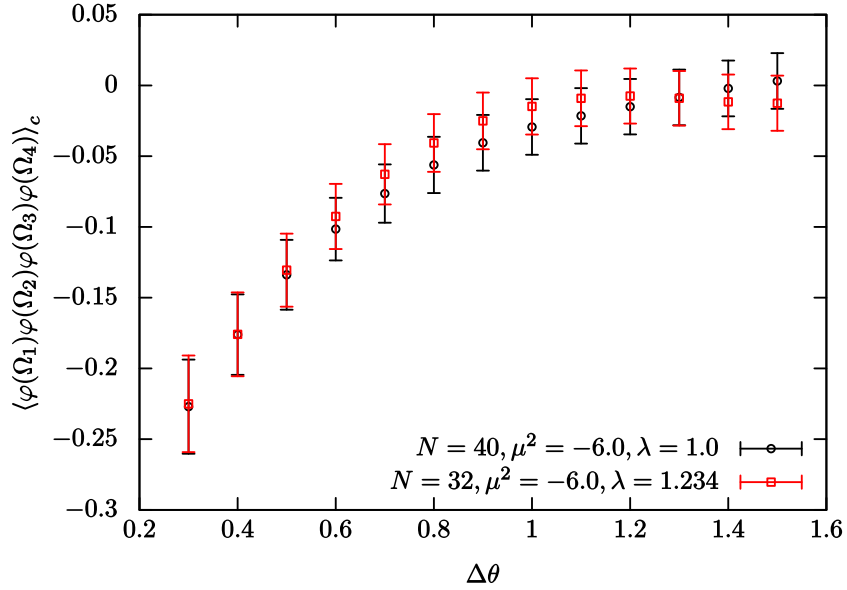


Figure 7: $\langle \varphi(\Omega_1)\varphi(\Omega_2)\varphi(\Omega_3)\varphi(\Omega_4) \rangle_c$ at $N = 40$, $\mu^2 = -6.0$, and $\lambda = 1.0$ is plotted against $\Delta\theta$, where circles represent the data. $\zeta'^2_{32 \rightarrow 40} \langle \varphi(\Omega_1)\varphi(\Omega_2)\varphi(\Omega_3)\varphi(\Omega_4) \rangle_c$ with $\zeta'^2_{32 \rightarrow 40} = 1.275$ at $N = 32$, $\mu^2 = -6.0$, and $\lambda = 1.234$ is also plotted against $\Delta\theta$, where squares represent the data.

$\lambda = 1.0$ if the former are multiplied by a constant $\zeta'_{32 \rightarrow 40} = \frac{Z(40)}{Z(32)} = 1.129(8)$ and that this is not the case for the data for $N = 32$ and $\lambda = 1.0, 2.0$. In Fig.6, we plot $\langle \varphi(\Omega_1)\varphi(\Omega_2) \rangle$ at $N = 40$ and $\lambda = 1.0$ and $\zeta'_{32 \rightarrow 40} \langle \varphi(\Omega_1)\varphi(\Omega_2) \rangle$ at $N = 32$ and $\lambda = 1.234$ against $\Delta\theta$. As in the previous section, we see that the data for $N = 32$ agree nicely with the ones for $N = 40$. This implies that the renormalized 2-point functions at $N = 32$ and $N = 40$ agree.

Furthermore, in Fig.7, we plot $\langle \varphi(\Omega_1)\varphi(\Omega_2)\varphi(\Omega_3)\varphi(\Omega_4) \rangle_c$ at $N = 40$ and $\lambda = 1.0$ and $\zeta'^2_{32 \rightarrow 40} \langle \varphi(\Omega_1)\varphi(\Omega_2)\varphi(\Omega_3)\varphi(\Omega_4) \rangle_c$ at $N = 32$ and $\lambda = 1.234$ against $\Delta\theta$. We again see a nice agreement between the data for $N = 32$ and the ones for $N = 40$, which means that the renormalized connected 4-point functions at $N = 32$ agree with those at $N = 40$.

The above results strongly suggest that the theory is also nonperturbatively renormalized by tuning λ in the sense that the renormalized correlation functions are independent of N .

The results in the previous and present sections imply that the theory is renormalized by tuning a parameter; namely, it is universal up to a parameter fine-tuning.

4 Critical behavior of correlation functions

In this section, we examine the 2-point and 4-point correlation functions on the phase boundary. We fix N at 24 in this section.

We introduce a stereographic projection defined by

$$z = R \tan \frac{\theta}{2} e^{i\varphi} , \quad (4.1)$$

which maps a sphere with the radius R to the complex plane. Here we fix R at 1 without loss of generality. We calculate the 2-point correlation function

$$\langle \varphi(z_m)\varphi(1) \rangle \quad (4.2)$$

and the connected 4-point correlation function

$$\langle \varphi(z_m)\varphi(1)\varphi(e^{i\frac{\pi}{3}})\varphi(e^{i\frac{5\pi}{3}}) \rangle_c , \quad (4.3)$$

where

$$z_m = \tan \left[\frac{1}{2} \left(\frac{\pi}{2} + 0.1m \right) \right] \quad (4.4)$$

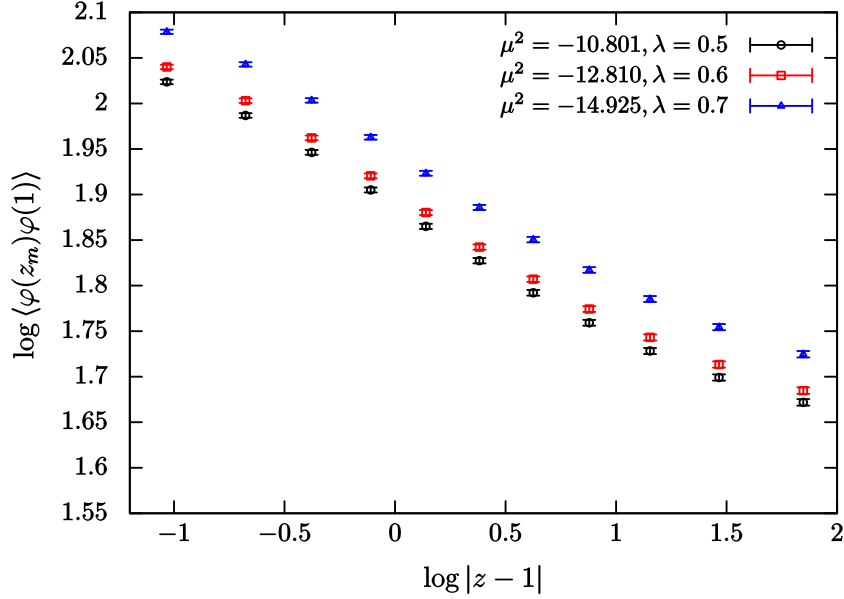


Figure 8: $\log\langle\varphi(z_m)\varphi(1)\rangle$ at $N = 24$ is plotted against $\log|z - 1|$. The data for $(\mu^2, \lambda) = (-10.801, 0.5)$, $(-12.810, 0.6)$, $(-14.925, 0.7)$ are represented by the circles, the squares, and the triangles, respectively.

with m taken from 1 to 15. See Fig. 1 with $\hat{\varphi} = \pi/3$.

The renormalized 2-point correlation function $\langle\varphi_r(z_m)\varphi_r(1)\rangle$ and the renormalized connected 4-point correlation function $\langle\varphi_r(z_m)\varphi_r(1)\varphi_r(e^{i\frac{\pi}{3}})\varphi_r(e^{i\frac{5\pi}{3}})\rangle_c$ are defined by

$$\langle\varphi(z_m)\varphi(1)\rangle = Z\langle\varphi_r(z_m)\varphi_r(1)\rangle, \quad (4.5)$$

$$\langle\varphi(z_m)\varphi(1)\varphi(e^{i\frac{\pi}{3}})\varphi(e^{i\frac{5\pi}{3}})\rangle_c = Z^2\langle\varphi_r(z_m)\varphi_r(1)\varphi_r(e^{i\frac{\pi}{3}})\varphi_r(e^{i\frac{5\pi}{3}})\rangle_c. \quad (4.6)$$

Here, in order to see a connection to a CFT, we use a log-log plot. We plot $\log\langle\varphi(z_m)\varphi(1)\rangle$ and $\log\langle\varphi(z_m)\varphi(1)\varphi(e^{i\frac{\pi}{3}})\varphi(e^{i\frac{5\pi}{3}})\rangle_c$ against $\log|z-1|$ for $(\mu^2, \lambda) = (-10.801, 0.5)$, $(-12.810, 0.6)$, $(-14.925, 0.7)$ in Figs.8 and 9, respectively.

We also define the susceptibility χ that is an order parameter for the Z_2 symmetry by

$$\chi = \left\langle \left(\frac{1}{N} \text{Tr} \Phi \right)^2 \right\rangle - \left\langle \frac{1}{N} |\text{Tr} \Phi| \right\rangle^2. \quad (4.7)$$

In Fig.10, we plot χ against $-\mu^2$ for each value of λ , 0.5, 0.6, 0.7. The critical values of $-\mu^2$, $-\mu_c^2$, that give the peaks of χ correspond to the phase transition points where symmetry breaking of the Z_2 symmetry occurs: the Z_2 symmetry is broken for $-\mu^2 > -\mu_c^2$, while it is unbroken for $-\mu^2 < -\mu_c^2$. We find that peaks of χ for $\lambda = 0.5, 0.6, 0.7$ exist around $\mu^2 = -10.8, -12.8, -14.8$, respectively. We tune the values of μ^2 around the

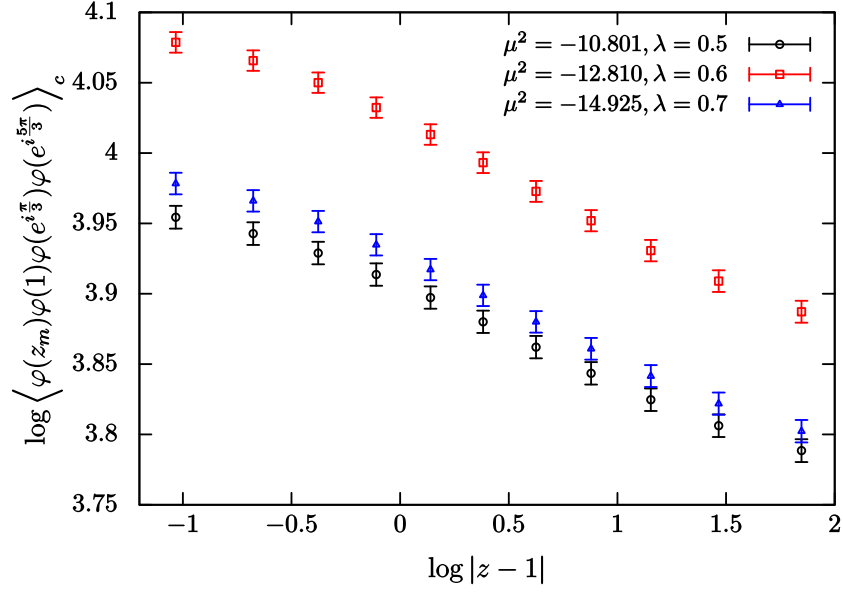


Figure 9: $\log\langle\varphi(z_m)\varphi(1)\varphi_r(e^{i\frac{\pi}{3}})\varphi_r(e^{i\frac{5\pi}{3}})\rangle_c$ at $N = 24$ is plotted against $\log|z - 1|$. The data for $(\mu^2, \lambda) = (-10.801, 0.5), (-12.810, 0.6), (-14.925, 0.7)$ are represented by the circles, the squares, and the triangles, respectively.

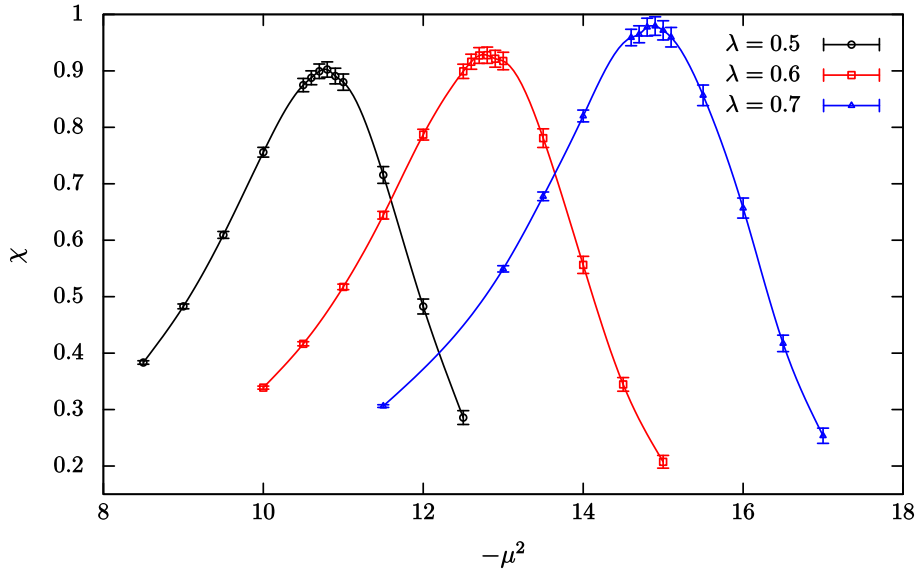


Figure 10: The susceptibility χ at $N = 24$ is plotted against $-\mu^2$. The data for $\lambda = 0.5, 0.6, 0.7$ are represented by the circles, the squares, and the triangles, respectively. The peaks of χ for $\lambda = 0.5, 0.6, 0.7$ exist around $\mu^2 = -10.8, -12.8, -14.8$, respectively.

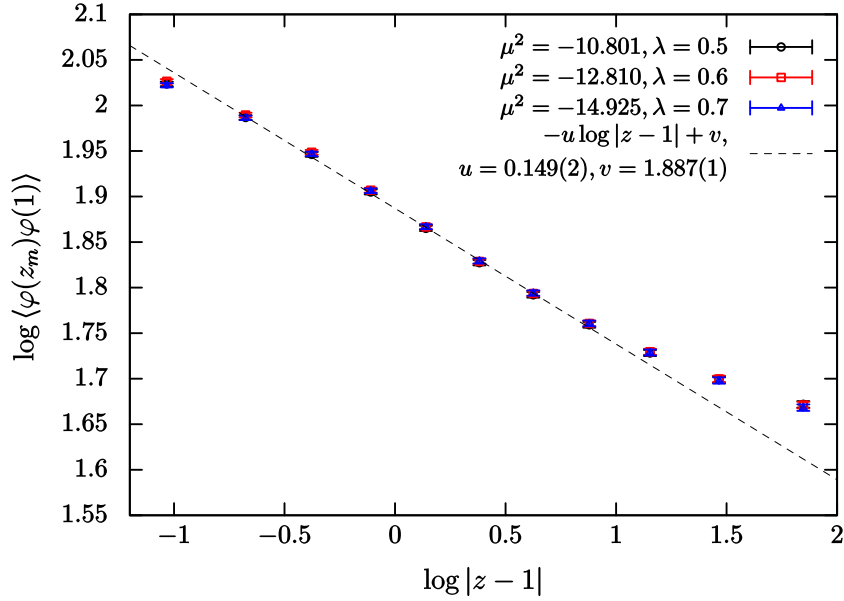


Figure 11: $\log\langle\varphi(z_m)\varphi(1)\rangle$ at $N = 24$ is plotted against $\log|z - 1|$. The data for $(\mu^2, \lambda) = (-10.801, 0.5)$ are the same as in Fig. 8. The data for $(\mu^2, \lambda) = (-12.810, 0.6), (-14.925, 0.7)$ are simultaneously shifted by $\alpha_{0.6 \rightarrow 0.5} = -0.015(1)$ and $\alpha_{0.7 \rightarrow 0.5} = -0.056(1)$, respectively, in the vertical direction. The data for $(\mu^2, \lambda) = (-10.801, 0.5), (-12.810, 0.6), (-14.925, 0.7)$ are represented by the circles, the squares, and the triangles, respectively. The dashed line is a fit of seven data points (from the second point to the eighth point) of $\log\langle\varphi(z_m)\varphi(1)\rangle$ at $(\mu^2, \lambda) = (-10.801, 0.5)$ to $-u \log|z - 1| + v$ with $u = 0.149(2)$ and $v = 1.887(1)$.

above values such that the 2-point and 4-point correlation functions for different λ agree up to a wave function renormalization. We shift the data of the 2-point correlation functions for $(\mu^2, \lambda) = (-12.810, 0.6), (-14.925, 0.7)$ simultaneously in the vertical direction by $\alpha_{0.6 \rightarrow 0.5} = \log[Z(\lambda = 0.5)/Z(\lambda = 0.6)] = -0.015(1)$ and $\alpha_{0.7 \rightarrow 0.5} = -0.056(1)$, respectively, and plot the shifted data in Fig.11. We also shift the data of the 4-point correlation functions for $(\mu^2, \lambda) = (-12.810, 0.6), (-14.925, 0.7)$ simultaneously by $2\alpha_{0.6 \rightarrow 0.5}$ and $2\alpha_{0.7 \rightarrow 0.5}$, respectively, and plot the shifted data in Fig.12. We see a good agreement of both the shifted 2-point and 4-point correlation functions. These shifts correspond to a wave function renormalization. Furthermore, we see that the above tuned values of μ^2 are consistent with the critical values of μ^2 read off from Fig.10. Thus, the agreement of the correlation functions implies that the theories are universal on the phase boundary as in ordinary field theories. We do not see the above agreement of the correlation functions in either the UV region with $m = 1, 2$, or the IR region with $m = 14, 15$. We consider the disagreement in

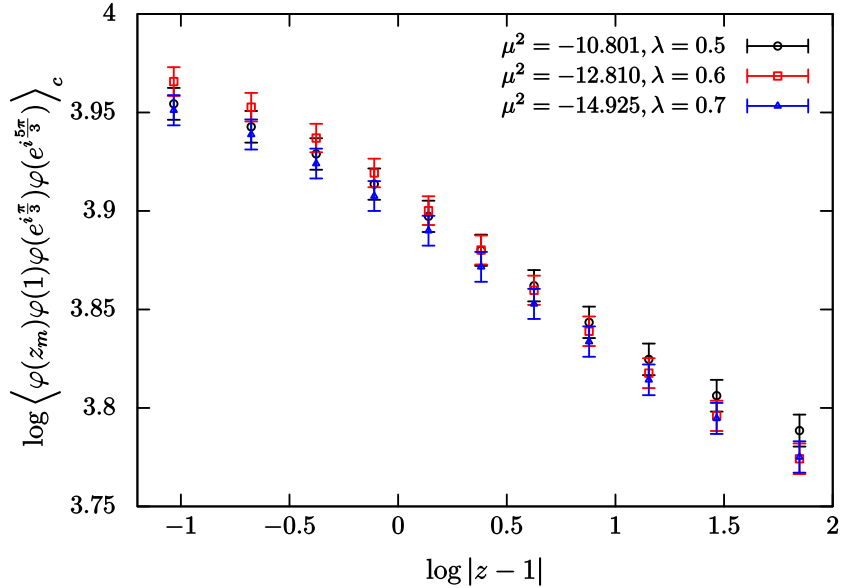


Figure 12: $\log\langle\varphi(z_m)\varphi(1)\varphi(e^{i\frac{\pi}{3}})\varphi(e^{i\frac{5\pi}{3}})\rangle_c$ at $N = 24$ is plotted against $\log|z - 1|$. The data for $(\mu^2, \lambda) = (-10.801, 0.5)$ are the same as in Fig. 9, while the data for $(\mu^2, \lambda) = (-12.810, 0.6), (-14.925, 0.7)$ are simultaneously shifted by $2\alpha_{0.6 \rightarrow 0.5}$ and $2\alpha_{0.7 \rightarrow 0.5}$, respectively, in the vertical direction. The data for $(\mu^2, \lambda) = (-10.801, 0.5), (-12.810, 0.6), (-14.925, 0.7)$ are represented by the circles, the squares, and the triangles, respectively.

the latter region to be caused by an IR cutoff that is introduced when the theory on the fuzzy sphere is mapped to a theory on the plane with infinite volume.

Finally, we examine a connection of the present theory to a CFT. In Fig.11, we fit seven data points ($m = 4, \dots, 10$) of $\log\langle\varphi(z_m)\varphi(1)\rangle$ at $(\mu^2, \lambda) = (-10.801, 0.5)$ to $-u \log|z-1| + v$ and obtain $u = 0.149(2)$ and $v = 1.887(1)$. This implies that the 2-point correlation function behaves as

$$\langle\varphi(z)\varphi(1)\rangle = \frac{e^v}{|z-1|^u} \quad (4.8)$$

for $m = 4, \dots, 10$. In CFTs, the 2-point correlation function behaves as

$$\langle\mathcal{O}(z)\mathcal{O}(z')\rangle \sim \frac{1}{|z-z'|^{2\Delta}}, \quad (4.9)$$

where the Δ is the scaling dimension of the operator $\mathcal{O}(z)$. Thus, the theory on the phase boundary behaves as a CFT in the UV region. In the IR region with $11 \leq m \leq 13$, our 2-point correlation function deviates universally from that in the CFT. In addition, in a further UV region with $m = 3$, it also deviates universally. These deviations are considered

to be an effect of the UV/IR mixing. It is nontrivial that we observe the behavior of the CFT because field theories on noncommutative spaces are non-local ones.

5 Conclusion and discussion

In this paper, we have studied renormalization in the scalar field theory on the fuzzy sphere by Monte Carlo simulation. We showed that the 2-point and 4-point correlation functions in the disordered phase are made independent of the UV cutoff up to the wave function renormalization by tuning the mass parameter or the coupling constant. This strongly suggests that the theory can be renormalized nonperturbatively in the ordinary sense and that the theory is universal up to a parameter fine-tuning.

We also examined the 2-point and 4-point correlation functions on the phase boundary beyond which the Z_2 symmetry is spontaneously broken. We found that the 2-point and 4-point correlation functions at different points on the boundary agree up to the wave function renormalization. This implies that the critical theory is universal, which is consistent with the above universality in the disordered phase, because the phase boundary is obtained by a parameter fine-tuning. Furthermore, we observed that the 2-point correlation functions behave as those in a CFT at short distances and deviate universally from those at long distances. The latter is considered to be due to the UV/IR mixing.

The CFT that we observed at short distances seems to differ from the critical Ising model, because the value of u in (4.8) disagrees with 2Δ , where Δ is the scaling dimension of the spin operator, $1/8$. This suggests that the universality classes of the scalar field theory on the fuzzy sphere are totally different from those of an ordinary field theory³.

Indeed, it was reported in [5–9] that there exists a novel phase in the theory on the fuzzy sphere that is called the nonuniformly ordered phase [24, 25]. We hope to elucidate the universality classes by studying renormalization in the whole phase diagram.

Acknowledgements

Numerical computation was carried out on the XC40 at YITP at Kyoto University and FX10 at the University of Tokyo. The work of A.T. is supported in part by a Grant-in-Aid

³It should be noted that the scaling dimension that we obtained, $\Delta \simeq 0.075 = 3/40$, coincides with that of the spin operator in the tricritical Ising model, which is the $(4, 5)$ unitary minimal model.

for Scientific Research (No. 15K05046) from JSPS.

Appendix: Bloch coherent state and Berezin symbol

In this appendix, we summarize the basic properties of the Bloch coherent state [23] and the Berezin symbol [22].

We use a standard basis $|jm\rangle$ ($m = -j, -j+1, \dots, j$) for the spin- j ($= (N-1)/2$) representation of the $SU(2)$ algebra. The action of L_i on the basis is given by

$$\begin{aligned} L_{\pm}|jm\rangle &= \sqrt{(j \mp m)(j \pm m + 1)}|jm \pm 1\rangle, \\ L_3|jm\rangle &= m|jm\rangle, \end{aligned} \quad (\text{A.1})$$

where $L_{\pm} = L_1 \pm iL_2$. The highest-weight state $|jj\rangle$ is considered to correspond to the north pole. Thus, the state $|\Omega\rangle$ that corresponds to a point $\Omega = (\theta, \varphi)$ is obtained by acting a rotation operator on $|jj\rangle$:

$$|\Omega\rangle = e^{i\theta(\sin\varphi L_1 - \cos\varphi L_2)}|jj\rangle. \quad (\text{A.2})$$

(A.2) implies that

$$n_i L_i |\Omega\rangle = j |\Omega\rangle, \quad (\text{A.3})$$

where $\vec{n} = (\sin\theta \cos\varphi, \sin\theta \sin\varphi, \cos\theta)$. It is easy to show from (A.3) that $|\Omega\rangle$ minimizes $\sum_i (\Delta L_i)^2$ with $(\Delta L_i)^2$ being the standard deviation of L_i .

It is convenient to introduce the stereographic projection, $z = R \tan \frac{\theta}{2} e^{i\varphi}$. Then, (A.2) is rewritten as

$$|\Omega\rangle = e^{zL_-/R} e^{-L_3 \log(1+|z/R|^2)} e^{-\bar{z}L_+/R} |jj\rangle, \quad (\text{A.4})$$

which gives an explicit form of $|\Omega\rangle$ as

$$|\Omega\rangle = \sum_{m=-j}^j \binom{2j}{j+m}^{\frac{1}{2}} \left(\cos \frac{\theta}{2}\right)^{j+m} \left(\sin \frac{\theta}{2}\right)^{j-m} e^{i(j-m)\varphi} |jm\rangle. \quad (\text{A.5})$$

By using (A.5), one can easily show the following relations:

$$\langle \Omega_1 | \Omega_2 \rangle = \left(\cos \frac{\theta_1}{2} \cos \frac{\theta_2}{2} + e^{i(\varphi_2 - \varphi_1)} \sin \frac{\theta_1}{2} \sin \frac{\theta_2}{2} \right)^{2j}, \quad (\text{A.6})$$

$$|\langle \Omega_1 | \Omega_2 \rangle| = \left(\cos \frac{\chi}{2} \right)^{2j} \quad \text{with } \chi = \arccos(\vec{n}_1 \cdot \vec{n}_2), \quad (\text{A.7})$$

$$\frac{2j+1}{4\pi} \int d\Omega |\Omega\rangle \langle \Omega| = 1. \quad (\text{A.8})$$

(A.7) implies that the width of the Bloch coherent state is $\frac{R}{\sqrt{j}}$ for large j .

Denoting the Bloch coherent state $|\Omega\rangle$ by $|z\rangle$, we rewrite (A.5) and (A.8) as

$$|z\rangle = \left(\frac{z/R}{1 + |z/R|^2} \right)^j \sum_{m=-j}^j \binom{2j}{j+m}^{\frac{1}{2}} \frac{R^m}{z^m} |jm\rangle, \quad (\text{A.9})$$

$$\frac{2j+1}{4\pi} 4R^2 \int \frac{d^2z}{(1 + |z/R|^2)^2} |z\rangle \langle z| = 1, \quad (\text{A.10})$$

respectively.

The Berezin symbol for a matrix A with the matrix size $2j+1$ is defined by

$$\begin{aligned} f_A(\Omega) &= f_A(z, \bar{z}) \\ &= \langle \Omega | A | \Omega \rangle \\ &= \langle z | A | z \rangle. \end{aligned} \quad (\text{A.11})$$

By using (A.5), it is easy to show that

$$f_{[L_i, A]}(\Omega) = \mathcal{L}_i f_A(\Omega). \quad (\text{A.12})$$

(A.8) implies that

$$\frac{1}{N} \text{Tr}(A) = \int \frac{d\Omega}{4\pi} f_A(\Omega). \quad (\text{A.13})$$

The definition of the star product for A and B is

$$f_A \star f_B(\Omega) = f_A \star f_B(z, \bar{z}) = \langle \Omega | AB | \Omega \rangle = \langle z | AB | z \rangle. \quad (\text{A.14})$$

Here let us consider a quantity

$$\frac{\langle w | A | z \rangle}{\langle w | z \rangle}, \quad (\text{A.15})$$

which is holomorphic in z and anti-holomorphic in w . Then, one can deform this quantity as follows:

$$\begin{aligned} \frac{\langle w | A | z \rangle}{\langle w | z \rangle} &= e^{-w \frac{\partial}{\partial z}} \frac{\langle w | A | z + w \rangle}{\langle w | z + w \rangle} \\ &= e^{-w \frac{\partial}{\partial z}} e^{z \frac{\partial}{\partial w}} \frac{\langle w | A | w \rangle}{\langle w | w \rangle} \\ &= e^{-w \frac{\partial}{\partial z}} e^{z \frac{\partial}{\partial w}} \langle w | A | w \rangle \\ &= e^{-w \frac{\partial}{\partial z}} e^{z \frac{\partial}{\partial w}} f_A(w, \bar{w}). \end{aligned} \quad (\text{A.16})$$

Similarly, one obtains

$$\frac{\langle z|A|w\rangle}{\langle z|w\rangle} = e^{-\bar{w}\frac{\partial}{\partial z}} e^{\bar{z}\frac{\partial}{\partial \bar{w}}} f_A(w, \bar{w}) . \quad (\text{A.17})$$

By using (A.10), (A.16), and (A.17), one can express the star product as

$$\begin{aligned} f_A \star f_B(w, \bar{w}) &= \langle w|AB|w\rangle \\ &= \frac{2j+1}{4\pi} 4R^2 \int \frac{d^2z}{(1+|z/R|^2)^2} \frac{\langle w|A|z\rangle}{\langle w|z\rangle} \frac{\langle z|B|w\rangle}{\langle z|w\rangle} |\langle w|z\rangle|^2 \\ &= \frac{2j+1}{4\pi} 4R^2 \int \frac{d^2z}{(1+|z/R|^2)^2} (e^{-w\frac{\partial}{\partial z}} e^{z\frac{\partial}{\partial w}} f_A(w, \bar{w})) (e^{-\bar{w}\frac{\partial}{\partial \bar{z}}} e^{\bar{z}\frac{\partial}{\partial \bar{w}}} f_B(w, \bar{w})) |\langle w|z\rangle|^2 , \end{aligned} \quad (\text{A.18})$$

which indicates that the star product is noncommutative and non-local. Furthermore, one can easily show that in the $j \rightarrow \infty$ limit

$$\frac{2j+1}{4\pi} \frac{4R^2}{(1+|z/R|^2)^2} |\langle w|z\rangle|^2 \rightarrow \delta^2(z-w) . \quad (\text{A.19})$$

This implies that the star product coincides with the ordinary product in the $j \rightarrow \infty$ limit. Namely,

$$f_A \star f_B(w, \bar{w}) \rightarrow f_A(w, \bar{w}) f_B(w, \bar{w}) \quad (\text{A.20})$$

or

$$f_A \star f_B(\Omega) \rightarrow f_A(\Omega) f_B(\Omega) . \quad (\text{A.21})$$

We see from (A.12), (A.13), and (A.21) that the theory (2.1) reduces to that of (2.4) in the $N \rightarrow \infty$ limit at the classical level if one identifies $f_{\Phi}(\Omega)$ with $\phi(\Omega)$. However, the authors of [3, 4] showed that the one-loop effective action in (2.1) differs from that in (2.4) by finite and non-local terms since the UV cutoff N is kept finite in calculating loop corrections. This phenomenon is sometimes called the UV/IR anomaly.

References

- [1] M. R. Douglas and N. A. Nekrasov, Rev. Mod. Phys. **73**, 977 (2001) [hep-th/0106048].
- [2] S. Minwalla, M. Van Raamsdonk and N. Seiberg, JHEP **0002**, 020 (2000) [hep-th/9912072].
- [3] C. S. Chu, J. Madore and H. Steinacker, JHEP **0108**, 038 (2001) [hep-th/0106205].

- [4] H. C. Steinacker, Nucl. Phys. B **910**, 346 (2016) [arXiv:1606.00646 [hep-th]].
- [5] X. Martin, JHEP **0404**, 077 (2004) [hep-th/0402230].
- [6] M. Panero, JHEP **0705**, 082 (2007) [hep-th/0608202].
- [7] M. Panero, SIGMA **2**, 081 (2006) [hep-th/0609205].
- [8] F. Garcia Flores, X. Martin and D. O'Connor, Int. J. Mod. Phys. A **24**, 3917 (2009) [arXiv:0903.1986 [hep-lat]].
- [9] C. R. Das, S. Digal and T. R. Govindarajan, Mod. Phys. Lett. A **23**, 1781 (2008) [arXiv:0706.0695 [hep-th]].
- [10] K. Hatakeyama and A. Tsuchiya, PTEP **2017**, no. 6, 063B01 (2017) [arXiv:1704.01698 [hep-th]].
- [11] S. Kawamoto and T. Kuroki, JHEP **1506**, 062 (2015) [arXiv:1503.08411 [hep-th]].
- [12] S. Vaidya and B. Ydri, Nucl. Phys. B **671**, 401 (2003) [hep-th/0305201].
- [13] D. O'Connor and C. Saemann, JHEP **0708**, 066 (2007) [arXiv:0706.2493 [hep-th]].
- [14] V. P. Nair, A. P. Polychronakos and J. Tekel, Phys. Rev. D **85**, 045021 (2012) [arXiv:1109.3349 [hep-th]].
- [15] A. P. Polychronakos, Phys. Rev. D **88**, 065010 (2013) [arXiv:1306.6645 [hep-th]].
- [16] J. Tekel, Phys. Rev. D **87**, no. 8, 085015 (2013) [arXiv:1301.2154 [hep-th]].
- [17] C. Saemann, JHEP **1504**, 044 (2015) [arXiv:1412.6255 [hep-th]].
- [18] J. Tekel, JHEP **1410**, 144 (2014) [arXiv:1407.4061 [hep-th]].
- [19] J. Tekel, JHEP **1512**, 176 (2015) [arXiv:1510.07496 [hep-th]].
- [20] W. Bietenholz, F. Hofheinz and J. Nishimura, JHEP **0406**, 042 (2004) [hep-th/0404020].
- [21] H. Mejía-Díaz, W. Bietenholz and M. Panero, JHEP **1410**, 56 (2014) [arXiv:1403.3318 [hep-lat]].

- [22] F. A. Berezin, *Commun. Math. Phys.* **40**, 153 (1975).
- [23] J. P. Gazeau. *Coherent states in quantum physics - 2009*. Weinheim, Germany: WileyVCH.
- [24] S. S. Gubser and S. L. Sondhi, *Nucl. Phys. B* **605**, 395 (2001) [hep-th/0006119].
- [25] J. Ambjorn and S. Catterall, *Phys. Lett. B* **549**, 253 (2002) [hep-lat/0209106].